Nano Research

Open Access

Research Article

Chirality inversion via van der Waals interactions to π–π stacking in non-equilibrium assembly within a narrow temperature range

Peiwen Chen[1,2], Kuo Fu[2], Xiangyang Zhang[2], Shengyin Zhao[1] ✉, Hongwei Wu[1] ✉, and Guofeng Liu[2] ✉

[1] *State Key Laboratory for Modification of Chemical Fibers and Polymer Materials, Science and Technology of Eco-Textile, Ministry of Education, Chemistry and Chemical Engineering, Donghua University, Shanghai 201620, China*
[2] *Shanghai Key Lab of Chemical Assessment and Sustainability, Chemical Science and Engineering, Advanced Research Institute, Tongji University, Shanghai 200092, China*

Cite this article: *Nano Research*, **2025**, *18*, 94907095. https://doi.org/10.26599/NR.2025.94907095

ABSTRACT: Understanding the dynamic control of supramolecular chirality is essential for the development of advanced chiral materials. This study presents a system where solvent-induced self-assembly of ortho-pyridine-azo-cholesterol (o-PAzPCC) and temperature-regulated co-assembly with Cu^{2+} exhibit dynamic supramolecular chirality inversion. Dimethylsulfoxide (DMSO) and alcohol solvents induce the reverse assembly of o-PAzPCC monomers, leading to circular dichroism (CD) signal inversion. Notably, the chloro-bridged Cu^{2+}/o-PAzPCC co-assembly system demonstrates temperature-regulated chirality inversion within a narrow range (283 to 293 K). At 283 K, van der Waals forces drive the formation of non-equilibrium nanosheet structures (Agg I) with positive CD absorption at 390 nm. At 293 K, π−π stacking interactions promote equilibrium nanoribbon structures (Agg III) with negative CD absorption at 440 nm wavelength. Increasing the temperature from 283 K can induce a transformation of the nanosheet structures to nanoflower structures (Agg II), characterized by positive CD absorption at 440 nm. The chirality inversion can be finely tuned by adjusting the concentrations and ultrasonication time. This work enhances our understanding of chiral assembly processes and their chirality transmission mechanisms, advancing the development of chiral supramolecular materials for applications in biological systems.

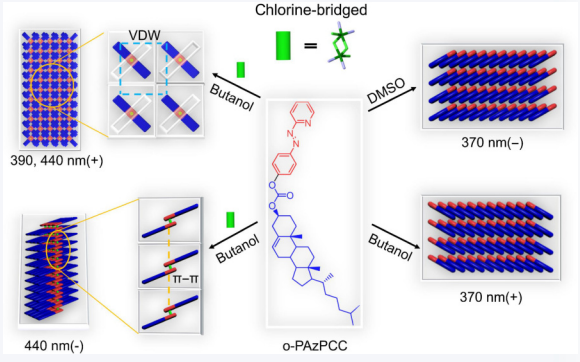

KEYWORDS: supramolecular chirality inversion, non-equilibrium self-assembly, chloro-bridged bond, coordinated supramolecular polymer, π−π stacking

1 Introduction

Building assembly nanostructures with tunable supramolecular chirality offers promising opportunities in various fields, including chiroptical switches, asymmetric catalysis, chiral recognition, biomedical optics, and beyond [1–8]. Precisely controlling dynamic supramolecular chirality is crucial for understanding chiral transmission and amplification in chemical self-assembly processes, which in turn guides the development of multifunctional chiral nanomaterials. Due to their inherent dynamic properties, small molecules can self-assemble into complex architectures through non-covalent interactions such as hydrogen bonding, π–π stacking, metal coordination, and van der Waals forces [9–16]. These interactions involve reversible processes of assembly, disassembly, and reassembly, allowing the resulting structures and corresponding properties to be tuned by varying physical conditions or external stimuli [17–22]. The flexibility and dynamic nature of supramolecular materials enable the creation of multifunctional and tunable systems that can adapt to changing conditions or stimuli. Research has shown that factors such as solvents, achiral additives, pH, light, and temperature significantly influence the outcomes of self-assembly. The artificial development of multifunctional materials that respond to external stimuli faces challenges due to the inherent environmental constraints within biological systems [23–28]. Temperature-responsive supramolecular systems may hold greater value in this context.

Received: August 29, 2024; **Revised:** October 16, 2024
Accepted: October 27, 2024

✉Address correspondence to Shengyin Zhao, syzhao8@dhu.edu.cn; Hongwei Wu, wuhongwei@dhu.edu.cn; Guofeng Liu, liuguofeng@tongji.edu.cn

However, achieving precise temperature-responsiveness and dynamic chirality inversion often requires higher temperatures or longer timescales, which limits their applicability in biological systems. Further exploration is needed to develop polymorphic chiral supramolecular systems that can achieve precise and rapid chirality responses within a narrow temperature range, ideally around room temperature. Such systems would offer significant advantages in biomedical applications, including targeted drug delivery, bioimaging, and biosensing. By optimizing the dynamic transmission and chirality inversion at physiological temperatures, we can enhance the functionality and versatility of these materials, making them more suitable for biological and medical applications.

The construction of polymorphic chiral supramolecular materials relies heavily on molecular stacking with various types of weak intermolecular forces [23, 29, 30]. Supramolecular self-assembly is driven by the synergistic effects of noncovalent interactions, including hydrogen bonding, π–π stacking, and van der Waals forces. Typically, interaction energies for van der Waals forces range from 0.4 to 4 kJ/mol, while π–π interactions vary from 0 to 50 kJ/mol [31]. The photoluminescence properties of organic materials are significantly influenced by intermolecular interactions [32–36]. Li et al. demonstrated how heating can differentiate the effects of hydrogen bonding, π–π stacking, and van der Waals forces on emission properties, leveraging the varying strengths of these interactions. Additionally, Wang et al. introduced a thermodynamic control strategy for π-conjugated supramolecular polymers, facilitating a transition from kinetically favored parallel stacking to thermodynamically favored slipped stacking [37]. Temperature control enables precise differentiation between π–π stacking and van der Waals forces. The remaining challenge is how to leverage these energy differences to construct supramolecular systems based on van der Waals and π–π stacking interactions, thereby advancing the development of finely tunable supramolecular chirality in self-assembly systems.

In this work, one end of o-PAzPCC features a cholesterol moiety that provides multiple van der Waals interaction sites and facilitates excellent chiral self-assembly. The other end contains a conjugated pyridine azobenzene unit, which enables π–π stacking and coordination with metal cations (Scheme 1). In dimethylsulphoxide (DMSO), the o-PAzPCC units were induced to tilt upwards to the right by 2.36° with an interlayer spacing of 15.82 Å, while in alcohol solvents, the units were induced to tilt upwards to the left by 2.36° with an interlayer spacing of 15.88 Å. The opposite stacking modes of the two types of solvents resulted in circular dichroism (CD) inversion at 370 nm. When o-PAzPCC coordinates with Cu^{2+} to form chloro-bridged Cu^{2+}/o-PAzPCC building units, the co-assembly follows a temperature-induced nucleation-growth assembly mode. At 283 K, Cu^{2+}/o-PAzPCC nucleates via van der Waals forces and grows parallelly in four directions to form nanosheet structures with a positive CD signal at 390 nm. These nanosheets can interlock into nanoflower structures upon heating, showing a positive CD signal at 440 nm. At 298 K, Cu^{2+}/o-PAzPCC forms dimers through van der Waals forces from cholesterol, which nucleates via π–π stacking between benzene, growing unidirectionally along the *a*-axis to form nanoribbon structures with a negative CD signal at 440 nm. The chiral inversion temperature of this polymorphic supramolecular system is modulated by concentration and ultrasonic treatment. These structures exhibit excellent stability at room temperature. This system enables a dual-mode switch: heating silences the CD signal,

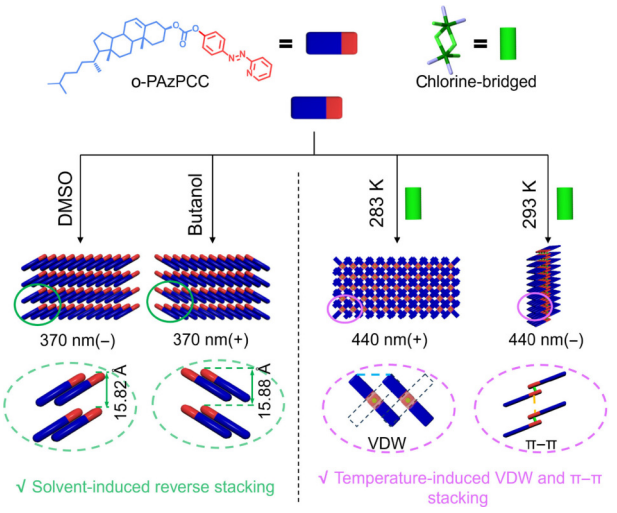

Scheme 1 DMSO and butanol induce reverse stacking of o-PAzPCC units, resulting in a mirror-image CD at 370 nm. Temperature-induced CD inversion of chloro-bridged Cu^{2+}/o-PAzPCC assemblies at 440 nm, van der Waals interactions between cholesterol yield positive signals structures at 283 K, and π–π stacking between benzene and pyridine yields negative signals structures at 293 K.

while ultrasonic activation at 268 K reveals a positive CD signal and at 298 K a negative CD signal. This Cu_2Cl_4 chlorine-bridge-based polymorphic assembly system not only allows for subtle modulation of supramolecular chirality inversion but also offers a platform for exploring the relationship between nanostructure and performance of dynamic supramolecular assemblies.

2 Results and discussion

2.1 Solvent-induced supramolecular chirality inversion

Ortho-pyridine-azo-cholesterol (o-PAzPCC) was synthesized and characterized following the procedures outlined in Figs. S1–S3 in the Electronic Supplementary Material (ESM). Previously, we demonstrated that cholesterol pyridine derivatives can self-assemble into self-supporting gels or suspensions in various organic solvents, exhibiting CD inversion [38–43]. In this study, we explored the self-assembly behavior of o-PAzPCC (16 mM) in 16 different organic solvents. As illustrated in Fig. 1(a) and Fig. S4 in the ESM, o-PAzPCC exhibited strong CD signals at 370 nm in DMSO and several alcoholic solvents, including isopropanol, butanol, hexanol, and ethanol, with absolute g_{abs} values reaching 10^{-3}. Remarkably, in DMSO, o-PAzPCC exhibited a negative CD signal, whereas in alcoholic solvents, it showed a positive CD signal. This solvent-induced supramolecular chirality inversion was confirmed to be free from interference by linear dichroism (Fig. S5 in the ESM). To gain further insight into the self-assembly process, we characterized the resultant nanostructures using scanning electron microscopy (SEM). The SEM images revealed that o-PAzPCC predominantly formed sheet-like aggregates, either orderly or disorderly, with sizes ranging from a few micrometers to several tens or even hundreds of micrometers (Figs. 1(b)–1(f) and Fig. S6 in the ESM). Our earlier studies on PAzPCC self-assembly indicated selectivity towards alcoholic solvents and DMSO [38, 39], likely due to the inherent polar structures of the sulfonyl and hydroxyl groups in the solvents. Although SEM images showed relatively uniform sheet-like structures at the microscopic level for assemblies with both positive

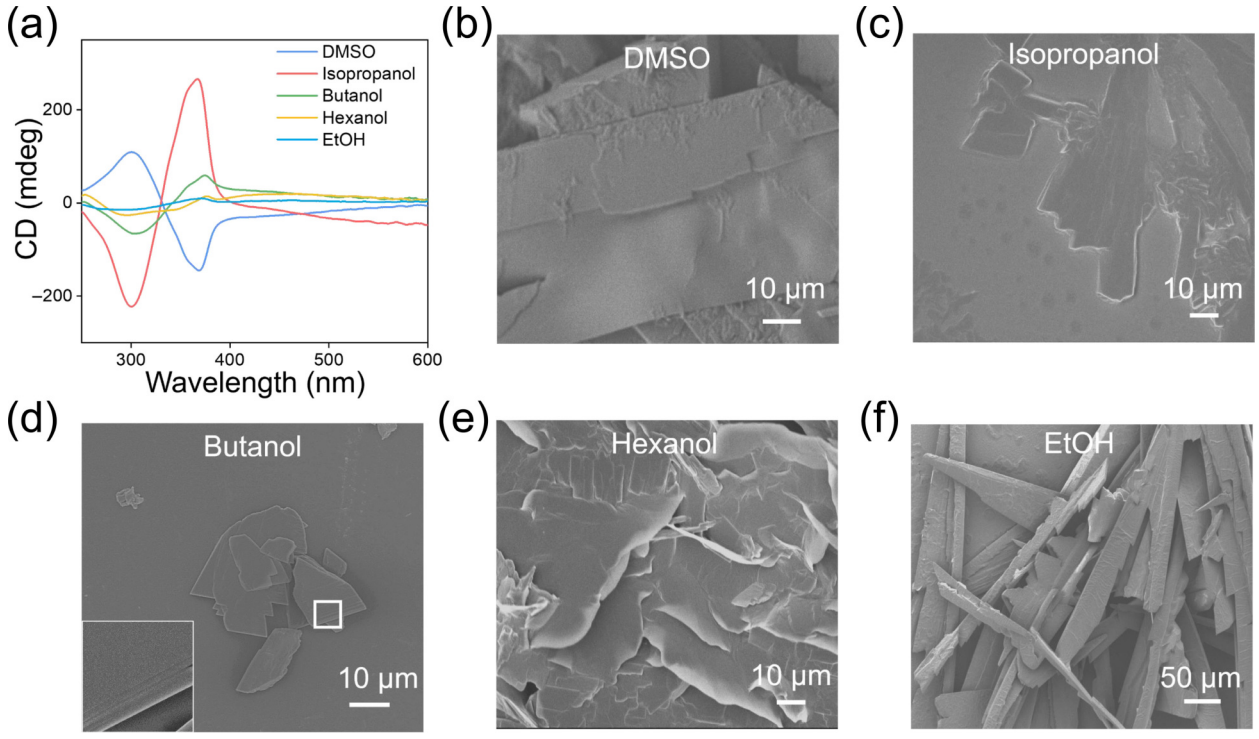

Figure 1 (a) CD spectra of o-PAzPCC assemblies obtained from different solvents. SEM images of o-PAzPCC assemblies obtained from (b) DMSO, (c) isopropanol, (d) butanol, (e) hexanol, and (f) EtOH. The concentration of o-PAzPCC was 16 mM.

and negative CD signals, further investigation is needed to elucidate the molecular mechanisms behind the solvent-induced supramolecular chirality inversion.

To further elucidate the mechanisms underlying solvent-induced supramolecular chirality inversion, crystal **1** of o-PAzPCC (20 mg) was obtained via slow evaporation of PX (3 mL) (Table S1 in the ESM). As shown in Fig. 2, crystal **1** features a layered stacking structure devoid of PX solvent molecules. The predominant intermolecular interactions are governed by van der Waals forces, characterized by three sets: C–H···H distances of 2.345 Å and C–H···O distances of 2.618 Å observed along the *c*-axis (Fig. 2(a)), and a C–H···H distance of 2.331 Å along the *a*-axis (Fig. 2(b)). The intermolecular distances measure 8.844 Å along the *c*-axis and 15.778 Å along the *a*-axis (Fig. 2(c)). The layers are tilted at a slip angle of 2.36°, leading to a calculated interlayer distance of 15.74 Å (Fig. 2(d)). Powder X-ray diffraction (XRD) analysis of the lyophilized o-PAzPCC powders self-assembled in DMSO and butanol revealed significant similarities to crystal **1** (Fig. 2(e)). The interplanar distances for the lyophilized powders were 15.82 and 6.05 Å for DMSO, and 15.88 and 6.05 Å for butanol, compared to 15.74 and 6.07 Å for crystal **1**. These findings suggest comparable stacking modes and properties across various crystal planes. Furthermore, the CD spectrum of crystal **1** exhibited a positive signal at 370 nm (Fig. S7 in the ESM), indicating a specific stacking mode of o-PAzPCC in butanol similar to crystal **1**, while suggesting an inverted stacking mode in DMSO (Fig. 2(f) and Fig. S8 in the ESM). Specifically, in butanol, o-PAzPCC displayed an upper left tilt with an interlayer distance of 15.88 Å, whereas in DMSO, it exhibited an upper right tilt with an interlayer distance of 15.82 Å. These solvent-induced two-directional stacking modes lead to inverted supramolecular chirality, resulting in mirror-image structures akin to enantiomers and CD inversion.

2.2 Temperature-directed chirality inversion of Cu^{2+}/o-PAzPCC cooperative assembly system

To modulate supramolecular chirality in our assembly system through metal coordination, we investigated the self-assembly of o-PAzPCC with various metal ions in different solvents (DMSO, butanol, and hexanol). o-PAzPCC was individually sonicated with six different metal ion solutions in each solvent, and the resulting assemblies were analyzed using CD spectroscopy. In DMSO, due to the formation of a mixed high-density ensemble between the o-PAzPCC assemblies and the highly viscous DMSO, CD signals resembling the o-PAzPCC assemblies without metal coordination were observed (Fig. S9(a) in the ESM), further mass spectrometry observations revealed a distinct peak for the [o-PAzPCC+H^+] at 612.41 (Fig. S10 in the ESM). This result suggested that DMSO's viscosity may hinder effective metal ion coordination. In contrast, in less polar solvents such as butanol and hexanol, assembly suspension showed effective chirality transfer when coordinated with Cu^{2+}, which has a strong coordination ability, eidenced by enhanced CD signals at 390 and 440 nm (Figs. S9(b) and S9(c) in the ESM). Of particular interest was the unique enhancement and transfer of supramolecular chirality observed with $CuCl_2$ in butanol. Subsequent SEM characterization provided additional insights into the nanostructures (Figs. S11–S13 in the ESM), revealing well-ordered aggregates formed in the systems based on the Cu^{2+}/o-PAzPCC complex.

Cu^{2+}/o-PAzPCC assemblies were prepared at 283 and 293 K, respectively. At both temperatures, Cu^{2+} rapidly disrupted the pre-existing chiral assemblies and slowed the formation of Cu^{2+}/o-PAzPCC co-assemblies (Figs. 3(a) and 3(b)). Notably, assemblies prepared at these two temperatures exhibited partially inverted supramolecular chirality. At 283 K, Cu^{2+}/o-PAzPCC co-assemblies exhibited positive CD signals at 390 and 440 nm with no significant

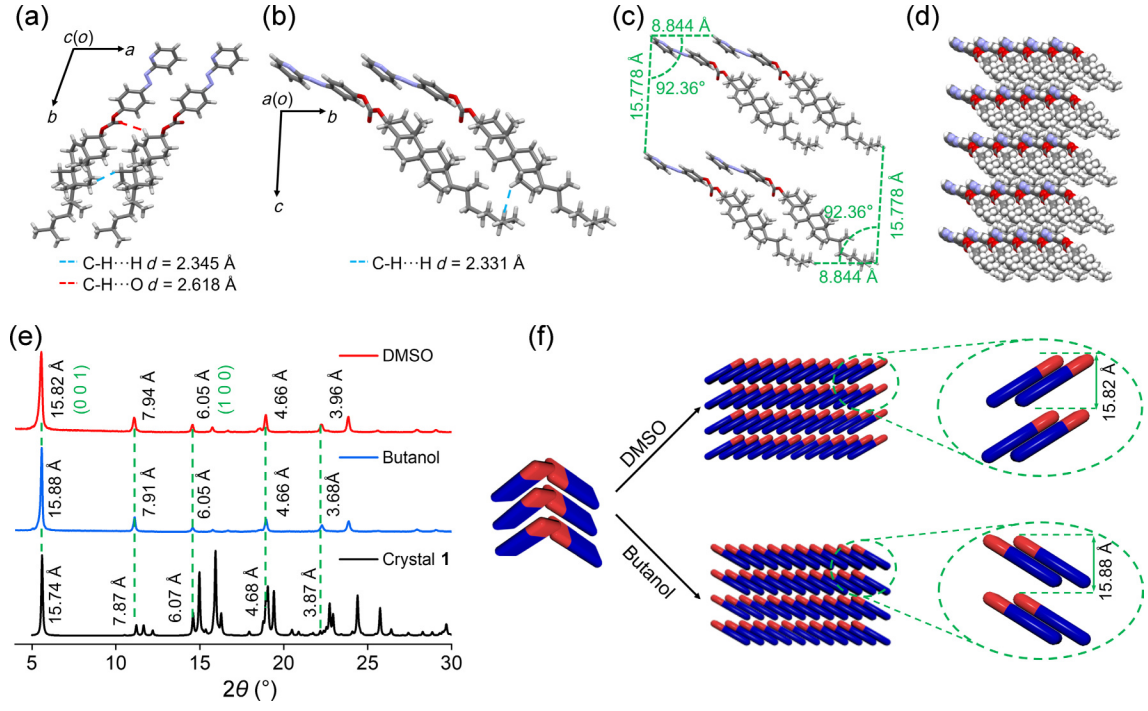

Figure 2 (a) Stacking and forces of crystal **1** along the *c*-axis. (b) Stacking and forces of crystal **1** along the *a*-axis. (c) Interlayer molecular distance and slip angles of crystal **1**. (d) Stacking model of crystal **1**. (e) XRD spectra of crystal **1** (black line), o-PAzPCC self-assembly from butanol (blue line), and DMSO (red line). (f) Schematic diagram of o-PAzPCC self-assembly in DMSO and butanol.

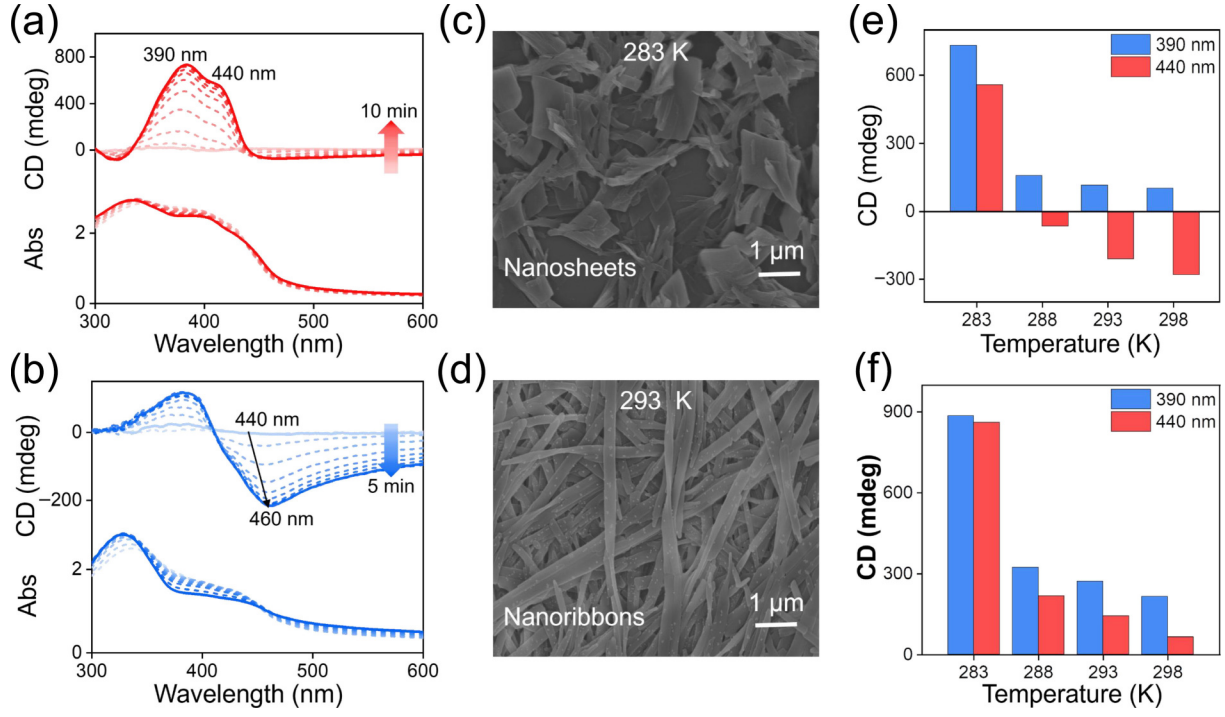

Figure 3 CD and corresponding UV–vis spectra of co-assembly of Cu^{2+}/o-PAzPCC obtained from butanol at (a) 283 K and (b) 293 K. SEM images of co-assembly of Cu^{2+}/o-PAzPCC obtained from butanol at (c) 283 K and (d) 293 K. Effect of temperature and sonication time on CD of co-assembly of Cu^{2+}/o-PAzPCC obtained from butanol during preparation with ultrasound for (e) 3 s and (f) 20 s. The concentration of Cu^{2+}/o-PAzPCC was 8 mM.

shifts in wavelength. In contrast, at 293 K, the co-assemblies showed a weaker positive CD signal at 390 nm and a negative CD signal at 440 nm, with a wavelength shift to 460 nm as the assembly developed, along with corresponding changes in ultraviolet (UV) absorption. SEM characterization revealed distinct morphologies of the assemblies prepared at 283 and 293 K (Figs. 3(c) and 3(d)). At 283 K, the assemblies appeared as dispersed, non-aggregated nanosheet structures, while at 293 K, they formed uniform nanoribbons. The infrared (IR) spectra of these assemblies are shown in Fig. S14(a) in the ESM. Compared to o-PAzPCC, the characteristic peaks of pyridine nitrogen shifted from 1586 to 1607 cm^{-1}, and azo peaks shifted from 1245 to 1268 cm^{-1} [44].

These shifts are attributed to charge transfer induced by Cu^{2+} coordination [45]. Additionally, the carbonate bond peak shifted from 1762 to 1744 cm^{-1}, indicating weaker interactions at the carbonate bond positions [46]. Changes in the IR peaks of $-CH_3$ and $-CH_2$ groups were also observed. The similarity in IR spectra between the two co-assemblies suggests that the chirality inversion is likely due to different stacking modes rather than variations in the Cu^{2+}/o-PAzPCC building blocks.

UV–visible (UV–vis) titration experiments confirmed that the optimal stoichiometry of Cu^{2+} to o-PAzPCC was 1: 1 (Fig. S14(b) in the ESM), indicating a structural ratio of 1:1 for the co-assembled units [47]. The self-assembly process involves both assembly and disassembly stages. The formation of Cu^{2+}/o-PAzPCC co-assemblies was gradual, allowing for the study of their growth kinetics (Figs. 3(a) and 3(b)). Assemblies with varying supramolecular chirality were observed after 10 min at 283 K and 5 min at 293 K, demonstrating the impact of temperature on reaching non-equilibrium and equilibrium states. At 283 K, the co-assemblies exhibited positive CD signals, which converted to negative CD signals at 440 nm after equilibration at 303 K (Fig. S15 in the ESM). Furthermore, increasing the concentration of Cu^{2+}/o-PAzPCC extended the time required for CD signal inversion, suggesting that the negative CD signals at 440 nm correspond to the thermodynamic equilibrium state [48–52]. This highlights the dynamic interplay between non-equilibrium and equilibrium states within the supramolecular assemblies [18, 19, 53].

The supramolecular chirality of the Cu^{2+}/o-PAzPCC assembly system finely tuned by competitive kinetics and thermodynamics. Beyond temperature, conditions for the preparation of assemblies such as ultrasonic duration and concentration affect the final chiral expression (Figs. S16 and S17 in the ESM). Non-equilibrium assemblies were classified as Agg I (390 nm, positive CD signal, nanosheets) and Agg II (440 nm, positive CD signal, nanoflowers), while the equilibrium assembly was classified as Agg III (440 nm, negative CD signal, nanoribbons). In the Cu^{2+}/o-PAzPCC (8 mM) system, the CD spectra growth rate increased with higher temperature (Fig. S17 in the ESM). Ultrasonication for 20 s enhanced the growth of non-equilibrium Agg I and Agg II (Figs. 3(e) and 3(f) and Fig. S16 in the ESM). Statistical analysis of the CD spectra growth curves after ultrasonication at 283 K showed that Agg I grew faster than Agg II after 3 s. However, after 20 s, Agg II grew faster than Agg I (Fig. S18 in the ESM). This indicates that longer ultrasonication times are more favorable for the growth of Agg II.

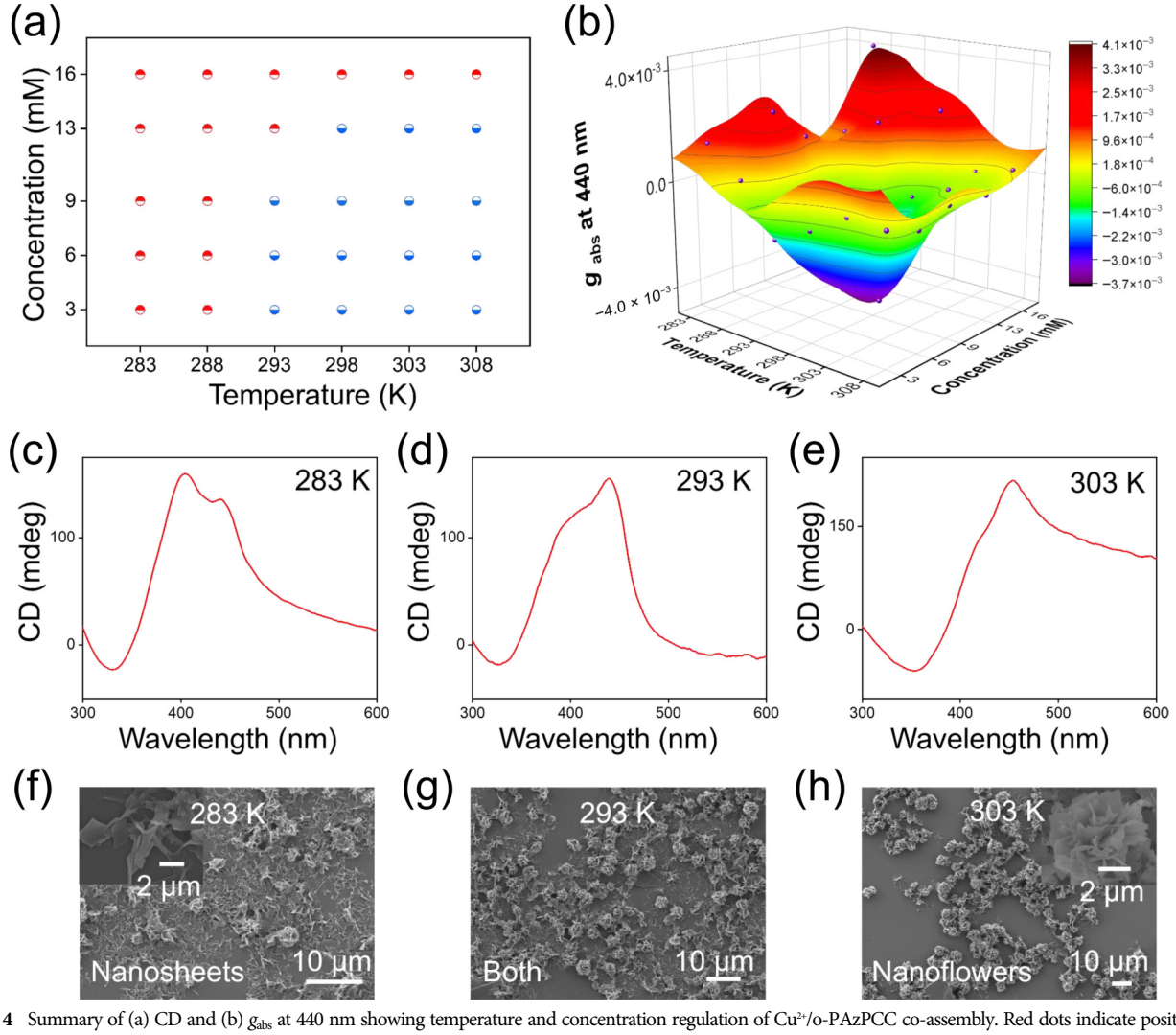

Figure 4 Summary of (a) CD and (b) g_{abs} at 440 nm showing temperature and concentration regulation of Cu^{2+}/o-PAzPCC co-assembly. Red dots indicate positive CD signals of non-equilibrium assembly Agg II, and blue dots indicate negative CD signals of equilibrium assembly Agg III. CD spectra of Cu^{2+}/o-PAzPCC co-assembly at (c) 283 K, (d) 293 K, and (e) 303 K. SEM images of Cu^{2+}/o-PAzPCC co-assembly at (f) 283 K, (g) 293 K, and (h) 303 K.

The study investigated the effects of temperature and concentration on both equilibrium and non-equilibrium products, using a fixed ultrasonication duration of 3 s (Fig. 4(a) and Figs. S19–S24 in the ESM). The regulation of the CD inversion temperature at 440 nm was influenced by concentration and ultrasonication time. Analysis of the absorption asymmetry factor (g_{abs}) showed that lower temperatures and higher concentrations promoted the formation of non-equilibrium products of Agg I and Agg II (Fig. 4(b)), which remained stable for extended periods at lower temperatures, specifically at 278 K (Fig. S25 in the ESM). The optimal conditions for preparing Agg III were found to be a Cu^{2+}/o-PAzPCC concentration of 8 mM at 298 K. Temperatures above this threshold led to the disassembly of the assemblies. This dynamic and thermodynamic control of supramolecular assembly was governed by the nucleation pathways influenced by the assembly conditions [54–56]. Consequently, whether the assembly formed a non-equilibrium or equilibrium structure was determined by these conditions. For example, Cu^{2+}/o-PAzPCC (8 mM) subjected to 3 s of ultrasonication at 283 K, and then either immediately varied from 283 to 298 K or maintained at 303 K, did not produce negative CD signals of Agg III (Figs. S26 and S27 in the ESM). However, temperature variations during CD growth affected the intensity of positive CD signals, with higher temperatures favoring CD growth at 440 nm (Agg II) (Figs. 4(c)–4(e)). SEM analysis demonstrated that as the temperature increased, the morphology evolved from nanosheet structures to stacked nanoflower shapes, with the nanosheet structures eventually vanishing (Figs. 4(f)–4(h)). The formation of nanoflower structures was entirely due to the stacking of nanosheets (Fig. 4(h)), indicating a transition from non-equilibrium Agg I to non-equilibrium Agg II. Optimizing growth temperature and extending ultrasonication time both promoted the hierarchical assembly of nanoflowers.

2.3 Dynamic chirality inversion mechanism in chloro-bridged Cu^{2+}/o-PAzPCC assembly system

Based on the analysis of the heating curve of CD spectra and the fitting of CD signals at 390 and 440 nm (Figs. 5(a) and 5(b) and Fig.

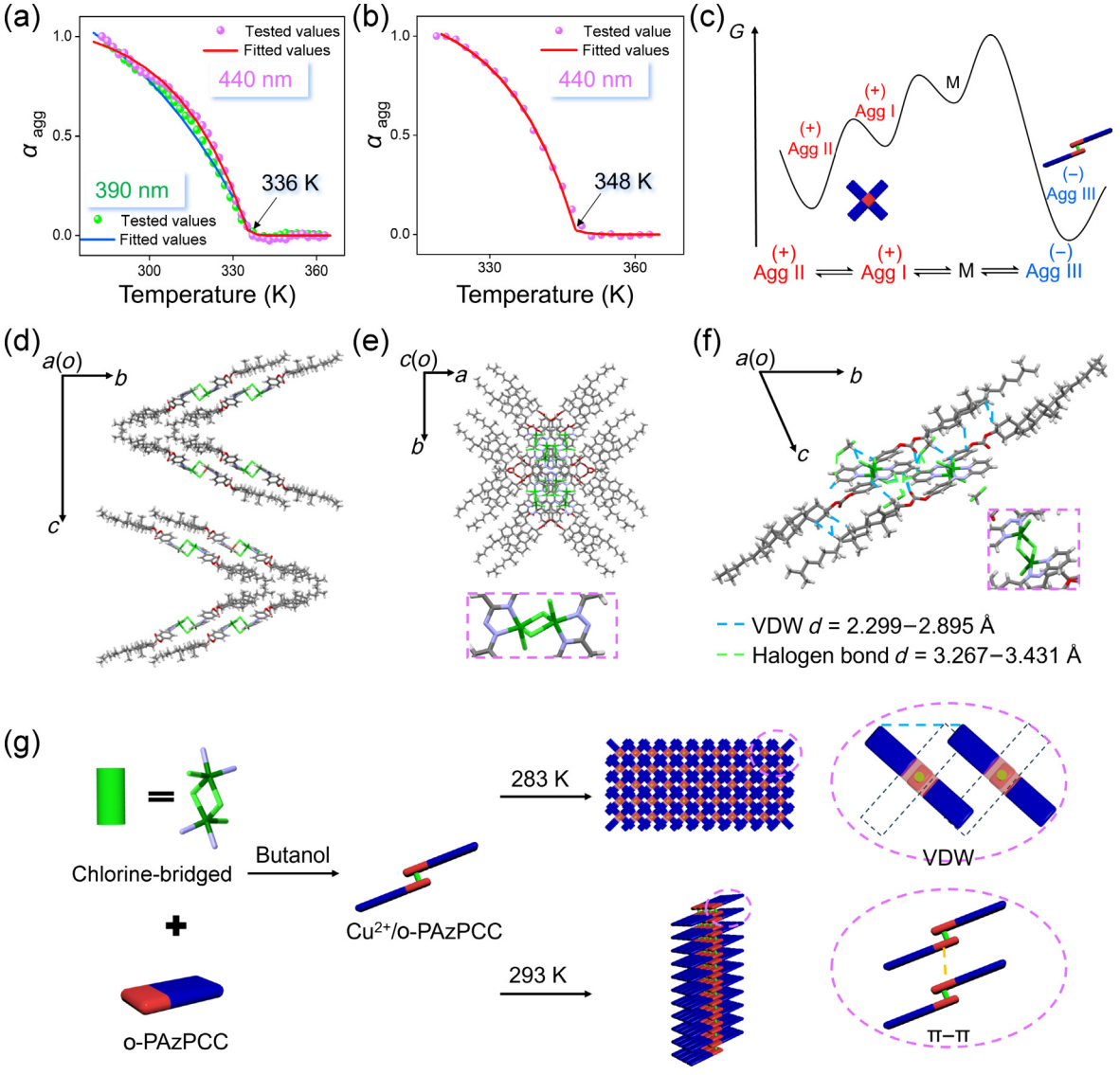

Figure 5 Fitted growth curves of (a) Agg I and Agg II and (b) Agg III. (c) Schematic Gibbs free energy landscape of co-assembly. Unit cell structure and internal forces of crystal **2** along the (d) *a*-axis and (e) *c*-axis. (f) Unit cell structure and internal forces of crystal **3** along the *a*-axis. (g) Schematic diagram of the supramolecular chirality inversion driven by van der Waals interactions and π–π stacking in chloro-bridged Cu^{2+}/o-PAzPCC assembly system.

S28 in the ESM), it was determined that Agg I, Agg II, and Agg III all followed a nucleation-growth assembly mechanism [57]. The critical growth temperatures were 336 K for both Agg I and Agg II, and 348 K for Agg III. The calculated enthalpy changes (ΔH) were −26236 J/mol for Agg I, −36423 J/mol for Agg II, and −70005 J/mol for Agg III, respectively. Entropy changes (ΔS) were −32.3 J/(mol·K) for Agg I, −62.5 J/(mol·K) for Agg II, and −155.3 J/(mol·K) for Agg III. And Gibbs free energies (ΔG) were −15396.8 J for Agg I, −15423.4 J for Agg II, and −15961.1 J for Agg III (Table S4 in the ESM). These results suggested that Agg I and Agg II were non-equilibrium hierarchical assemblies formed through homonuclear processes, with Agg II evolving from the stacking of Agg I. The significant changes in enthalpy and entropy values between the assemblies highlight the increasing stability and complexity of the hierarchical structures as they transition from Agg I to Agg III (Fig. 5(c)).

To gain deeper insights into the mechanism of chirality inversion, single crystals of the corresponding metal-coordinated complexes were cultured. Initially, o-PAzPCC (200 mg) and $CuCl_2$ (22 mg) were reacted in EtOH (20 mL) for 12 h to form Cu^{2+}/o-PAzPCC assemblies. The resulting product was then dissolved in dichloromethane (DCM) (20 mL) and allowed to evaporate naturally, yielding crystal **2** (Table S2 in the ESM). Over time, a portion of crystal **2** gradually transformed into crystal **3** (Table S3 in the ESM), corresponding to observed structural changes in the assemblies. Both crystals consist of building units with a 2:2 ratio of Cu^{2+} to o-PAzPCC, rather than 1:1 ratio. However, they differ in their unit cell compositions and stacking arrangements. Specifically, crystal **2** features four 2-unit building blocks arranged in two anti-parallel trumpet shapes along the *a*-axis (Fig. 5(d)) and crosswise pairs along the *c*-axis (Fig. 5(e)). Importantly, there are no interactions between the building units within this arrangement. In crystal **3**, the unit cell exhibits dimeric anti-parallel arrangements of Cu^{2+}/o-PAzPCC building units, primarily stabilized by weak intermolecular interactions involving the solvent DCM. These interactions include van der Waals forces ranging from 2.299 to 2.895 Å and halogen bonds spanning from 3.267 to 3.431 Å (Fig. 5(f)). The formation of dimers is chiefly driven by van der Waals interactions between cholesterols, potentially augmented by halogen bonding from DCM. Crystal **2** adopts a sheet-like metastable structure due to stacking in four perpendicular directions relative to the arrangement of its components. Stacking is facilitated by van der Waals forces (distances of 2.581 to 3.489 Å) between cholesterol and chlorine-bridged components. In contrast, crystal **3** forms ribbon-like structures along the *a*-axis, driven by π–π stacking interactions (distance of 3.381 Å) between benzene rings of the dimers (Figs. S29(b) and S30(b) in the ESM). These structural observations align with the SEM morphologies observed in Agg I and Agg III, as well as the observed redshift in CD signals during the growth of Agg III [58]. Figure 5(g) illustrates the sensitivity of Cu^{2+}/o-PAzPCC building units, constructed with chlorine bridges and o-PAzPCC, to assembly conditions in butanol at room temperature. At 283 K, these units stack into layered structures due to van der Waals interactions involving cholesterol. At 293 K, they form nanobelts via π–π interactions between benzene rings.

The Cu^{2+}/o-PAzPCC assembly system achieved precise control over supramolecular chirality by regulating kinetic factors during nucleation. This control enables the development of a temperature-sensitive supramolecular chiral ultrasound switch. When heated, the assemblies disassemble into Cu^{2+}/o-PAzPCC monomers. Upon cooling, these monomers reassemble into large micron-sized particles (approximately 100 micrometers), which exhibit CD silence (Fig. S31 in the ESM). When exposed to 3 s at temperatures of 268 and 298 K, these micron-sized particles exhibit distinct chiroptical activities: They produce positively CD-active Agg I (Figs. S31(b) and S31(c) in the ESM), Agg II, and negatively CD-active Agg III (Figs. S31(d) and S31(e) in the ESM). This temperature-sensitive ultrasound switch demonstrates rapid response and excellent repeatability (Fig. S31(f) in the ESM). Thus, the Cu^{2+}/o-PAzPCC system's ability to modulate nucleation kinetics allows for precise control over the chirality of supramolecular assemblies, leading to the development of a responsive ultrasound switch that can switch chiroptical properties depending on temperature changes.

3 Conclusions

In summary, we present a system where solvent-induced self-assembly of o-PAzPCC and temperature-modulated Cu^{2+}/o-PAzPCC co-assembly exhibit dynamic supramolecular chirality inversion. Solvents such as DMSO and alcohol induce chirality inversion in o-PAzPCC assemblies, attributed to solvent-induced reverse arrangements of o-PAzPCC motifs, as confirmed by single crystal and powder XRD analysis. The Cu^{2+}/o-PAzPCC co-assembly, based on chloride-bridging, follows a nucleation-growth assembly model. At 283 K, Cu^{2+}/o-PAzPCC nucleates and grows into non-equilibrium nanosheet structures (Agg I), characterized by positive CD absorption at 390 nm. This is driven by van der Waals interactions between the cholesterol moieties and the chlorine-bridged units. At 293 K, Cu^{2+}/o-PAzPCC transitions to dimers stabilized by van der Waals interactions and further assembles into nanoribbon structures (the equilibrium assembly of Agg III), which exhibit negative CD absorption at 440 nm, facilitated by π–π stacking interactions between benzene rings. Upon further heating, the nanosheet structures can transform into higher-order metastable nanoflower structures (the non-equilibrium assembly of Agg II) with positive CD at 440 nm. Leveraging these findings, we have developed a temperature-sensitive supramolecular chiral bidirectional switch. These insights deepen our understanding of chiral transmission in supramolecular assembly processes and provide opportunities for designing chiral supramolecular materials with tunable properties.

Electronic Supplementary Material: Supplementary material (including MS, NMR, UV–vis, CD, IR, and SEM measurements) is available in the online version of this article at https://doi.org/10.26599/NR.2025.94907095.

Data availability

All data needed to support the conclusions in the paper are presented in the manuscript and the Electronic Supplementary Material. Additional data related to this paper may be requested from the corresponding author upon request.

Acknowledgements

This research is supported by the National Natural Science Foundation of China (Nos. 22471198 and 22101208), the Fundamental Research Funds for the Central Universities, and the Program for Professors of Special Appointment (Eastern Scholar) at Shanghai Institutions of Higher Learning.

Declaration of competing interest

The authors declare no conflict of interest.

Author contribution statement

P. W. C.: Data curation, validation, writing the manuscript, experimental design. K. F. and X. Y. Z.: Data curation, validation, experimental design. S. Y. Z. and H. W. W.: Project administration, writing the manuscript. G. F. L.: Project administration, funding acquisition, writing the manuscript. All authors have approved the final manuscript.

Use of AI statement

None.

References

[1] Gong, Z. L.; Zhu, X. F.; Zhou, Z. H.; Zhang, S. W.; Yang, D.; Zhao, B.; Zhang, Y. P.; Deng, J. P.; Cheng, Y. X.; Zheng, Y. X. et al. Frontiers in circularly polarized luminescence: Molecular design, self-assembly, nanomaterials, and applications. *Sci. China Chem.* **2021**, *64*, 2060–2104.

[2] Yan, H. W.; He, Y. L.; Wang, D.; Han, T.; Tang, B. Z. Aggregation-induced emission polymer systems with circularly polarized luminescence. *Aggregate* **2023**, *4*, e331.

[3] Sang, Y. T.; Han, J. L.; Zhao, T. H.; Duan, P. F.; Liu, M. H. Circularly polarized luminescence in nanoassemblies: Generation, amplification, and application. *Adv. Mater.* **2020**, *32*, 1900110.

[4] Stachelek, P.; MacKenzie, L.; Parker, D.; Pal, R. Circularly polarised luminescence laser scanning confocal microscopy to study live cell chiral molecular interactions. *Nat. Commun.* **2022**, *13*, 553.

[5] Lu, X. Y.; Zhang, K.; Niu, X. K.; Ren, D. D.; Zhou, Z.; Dang, L. L.; Fu, H. R.; Tan, C. L.; Ma, L. F.; Zang, S. Q. Encapsulation engineering of porous crystalline frameworks for delayed luminescence and circularly polarized luminescence. *Chem. Soc. Rev.* **2024**, *53*, 6694–6734.

[6] Gong, Z. L.; Dan, T. X.; Chen, J. C.; Li, Z. Q.; Yao, J. N.; Zhong, Y. W. Boost the circularly polarized phosphorescence of chiral organometallic platinum complexes by hierarchical assembly into fibrillar networks. *Angew. Chem., Int. Ed.* **2024**, *63*, e202402882.

[7] Yang, D.; Han, J. L.; Sang, Y. T.; Zhao, T. H.; Liu, M. H.; Duan, P. F. Steering triplet-triplet annihilation upconversion through enantioselective self-assembly in a supramolecular gel. *J. Am. Chem. Soc.* **2021**, *143*, 13259–13265.

[8] Ren, C.; Sun, W. J.; Zhao, T. H.; Li, C. X.; Jiang, C. Y.; Duan, P. F. A single-enantiomer emitter enabled superstructural helix inversion for upconverting and downshifting luminescence with bidirectional circular polarization. *Angew. Chem., Int. Ed.* **2023**, *62*, e202315136.

[9] Liu, G. F.; Humphrey, M. G.; Zhang, C.; Zhao, Y. L. Self-assembled stereomutation with supramolecular chirality inversion. *Chem. Soc. Rev.* **2023**, *52*, 4443–4487.

[10] Wang, L.; Song, B.; Li, Y. M.; Gong, L. L.; Jiang, X.; Wang, M.; Lu, S.; Hao, X. Q.; Xia, Z. H.; Zhang, Y. et al. Self-assembly of metallo-supramolecules under kinetic or thermodynamic control: Characterization of positional isomers using scanning tunneling spectroscopy. *J. Am. Chem. Soc.* **2020**, *142*, 9809–9817.

[11] Sun, P. P.; Han, B. L.; Li, H. G.; Zhang, C. K.; Xin, X.; Dou, J. M.; Gao, Z. Y.; Sun, D. Real-time fluorescent monitoring of kinetically controlled supramolecular self-assembly of atom-precise Cu_8 nanocluster. *Angew. Chem., Int. Ed.* **2022**, *61*, e202200180.

[12] Long, Z. F.; Zheng, S. Y.; Zhou, W. Q.; Liu, G. F. Supramolecular chirality capture in solvent monomer-based co-assemblies via *in situ* photopolymerization. *Chem. Commun.* **2024**, *60*, 9054–9057.

[13] Zheng, S. Y.; Liu, G. F. Hierarchical self-assembly promoted circularly polarized luminescence enhancement and handedness inversion of metal-organic helicate. *CCS Chem.* **2024**, *6*, 2198–2209.

[14] Huang, Z. Z.; Jiang, T.; Wang, J.; Ma, X.; Tian, H. Real-time visual monitoring of kinetically controlled self-assembly. *Angew. Chem., Int. Ed.* **2021**, *60*, 2855–2860.

[15] Zhang, Q.; Crespi, S.; Toyoda, R.; Costil, R.; Browne, W. R.; Qu, D. H.; Tian, H.; Feringa, B. L. Stereodivergent chirality transfer by noncovalent control of disulfide bonds. *J. Am. Chem. Soc.* **2022**, *144*, 4376–4382.

[16] Shi, Z. T.; Wang, Q.; Yi, J. H.; Zhao, C. X.; Chen, S. Y.; Tian, H.; Qu, D. H. Encoding supramolecular chiral self-assembly with photo-controlled circularly polarized luminescence by overcrowded alkene-based Bis-PBI modulators. *Angew. Chem., Int. Ed.* **2022**, *61*, e202207405.

[17] Matern, J.; Dorca, Y.; Sánchez, L.; Fernández, G. Revising complex supramolecular polymerization under kinetic and thermodynamic control. *Angew. Chem., Int. Ed.* **2019**, *58*, 16730–16740.

[18] Kulkarni, C.; Korevaar, P. A.; Bejagam, K. K.; Palmans, A. R. A.; Meijer, E. W.; George, S. J. Solvent clathrate driven dynamic stereomutation of a supramolecular polymer with molecular pockets. *J. Am. Chem. Soc.* **2017**, *139*, 13867–13875.

[19] Sorrenti, A.; Leira-Iglesias, J.; Markvoort, A. J.; de Greef, T. F. A.; Hermans, T. M. Non-equilibrium supramolecular polymerization. *Chem. Soc. Rev.* **2017**, *46*, 5476–5490.

[20] Kumar, M.; George, S. J. Homotropic and heterotropic allosteric regulation of supramolecular chirality. *Chem. Sci.* **2014**, *5*, 3025–3030.

[21] Ji, H. H.; Wu, B.; Tian, E. Q.; Ren, C.; Jin, X.; Zhu, L. L.; Duan, P. F. Upconverting and downshifting circularly polarized luminescence in a superstructural helix. *Sci. China Chem.* **2024**, *67*, 2571–2577.

[22] Yang, F.; Yue, B. B.; Zhu, L. L. Light-triggered modulation of supramolecular chirality. *Chem.—Eur. J.* **2023**, *29*, e202203794.

[23] Zhang, Y. X.; Li, H.; Geng, Z. X.; Zheng, W. H.; Quan, Y. W.; Cheng, Y. X. Inverted circularly polarized luminescence behavior induced by helical nanofibers through chiral co-assembly from achiral liquid crystal polymers and chiral inducers. *ACS Nano* **2022**, *16*, 3173–3181.

[24] Arias, S.; Freire, F.; Calderón, M.; Bergueiro, J. Unexpected chiro-thermoresponsive behavior of helical poly(phenylacetylene)s bearing elastin-based side chains. *Angew. Chem., Int. Ed.* **2017**, *56*, 11420–11425.

[25] Kulkarni, C.; Mondal, A. K.; Das, T. K.; Grinbom, G.; Tassinari, F.; Mabesoone, M. F. J.; Meijer, E. W.; Naaman, R. Highly efficient and tunable filtering of electrons' spin by supramolecular chirality of nanofiber-based materials. *Adv. Mater.* **2020**, *32*, 1904965.

[26] Yan, J. L.; Ota, F.; San Jose, B. A.; Akagi, K. Chiroptical resolution and thermal switching of chirality in conjugated polymer luminescence via selective reflection using a double-layered cell of chiral nematic liquid crystal. *Adv. Funct. Mater.* **2017**, *27*, 1604529.

[27] Go, M. S.; Choi, H.; Kim, K. Y.; Moon, C. J.; Choi, Y.; Miyake, H.; Lee, S. S.; Jung, S. H.; Choi, M. Y.; Jung, J. H. Temperature-controlled helical inversion of asymmetric triphenylamine-based supramolecular polymers; difference of handedness at the micro-and macroscopic levels. *Org. Chem. Front.* **2019**, *6*, 1100–1108.

[28] Choi, H.; Heo, S.; Lee, S.; Kim, K. Y.; Lim, J. H.; Jung, S. H.; Lee, S. S.; Miyake, H.; Lee, J. Y.; Jung, J. H. Kinetically controlled Ag^+-coordinated chiral supramolecular polymerization accompanying a helical inversion. *Chem. Sci.* **2020**, *11*, 721–730.

[29] Wehner, M.; Würthner, F. Supramolecular polymerization through kinetic pathway control and living chain growth. *Nat. Rev. Chem.* **2020**, *4*, 38–53.

[30] Wehner, M.; Röhr, M. I. S.; Bühler, M.; Stepanenko, V.; Wagner, W.; Würthner, F. Supramolecular polymorphism in one-dimensional self-assembly by kinetic pathway control. *J. Am. Chem. Soc.* **2019**, *141*, 6092–6107.

[31] Liu, X. X.; Liao, Q. Y.; Yang, J.; Li, Z.; Li, Q. Q. Unveiling one-to-one correspondence between excited triplet states and determinate interactions by temperature-controllable blue-green-yellow afterglow. *Angew. Chem., Int. Ed.* **2023**, *62*, e202302792.
[32] Zhang, W.; Luo, Y.; Liu, C.; Yang, M. X.; Gou, J. X.; Huang, Y.; Ni, X. L.; Tao, Z.; Xiao, X. Supramolecular room temperature phosphorescent materials based on cucurbit[8]uril for dual detection of dodine. *ACS Appl. Mater. Interfaces* **2022**, *14*, 51429–51437.
[33] Garain, S.; Wagalgave, S. M.; Kongasseri, A. A.; Garain, B. C.; Ansari, S. N.; Sardar, G.; Kabra, D.; Pati, S. K.; George, S. J. Anion-π-induced room temperature phosphorescence from emissive charge-transfer states. *J. Am. Chem. Soc.* **2022**, *144*, 10854–10861.
[34] Singh, M.; Liu, K.; Qu, S. L.; Ma, H. L.; Shi, H. F.; An, Z. F.; Huang, W. Recent advances of cocrystals with room temperature phosphorescence. *Adv. Opt. Mater.* **2021**, *9*, 2002197.
[35] Kwon, M. S.; Lee, D.; Seo, S.; Jung, J.; Kim, J. Tailoring intermolecular interactions for efficient room-temperature phosphorescence from purely organic materials in amorphous polymer matrices. *Angew. Chem., Int. Ed.* **2014**, *53*, 11177–11181.
[36] Wu, H. Z.; Wang, D. L.; Zhao, Z.; Wang, D.; Xiong, Y.; Tang, B. Z. Tailoring noncovalent interactions to activate persistent room-temperature phosphorescence from doped polyacrylonitrile films. *Adv. Funct. Mater.* **2021**, *31*, 2101656.
[37] Wang, F.; Liao, R.; Wang, F. Pathway control of π-conjugated supramolecular polymers by incorporating donor-acceptor functionality. *Angew. Chem., Int. Ed.* **2023**, *62*, e202305827.
[38] Liu, G. F.; Sheng, J. H.; Teo, W. L.; Yang, G. B.; Wu, H. W.; Li, Y. X.; Zhao, Y. L. Control on dimensions and supramolecular chirality of self-assemblies through light and metal ions. *J. Am. Chem. Soc.* **2018**, *140*, 16275–16283.
[39] Yao, L. F.; Fu, K.; Wang, X. J.; He, M. L.; Zhang, W. N.; Liu, P. Y.; He, Y. P.; Liu, G. F. Metallophilic interaction-mediated hierarchical assembly and temporal-controlled dynamic chirality inversion of metal-organic supramolecular polymers. *ACS Nano* **2023**, *17*, 2159–2169.
[40] Liu, C. T.; Fu, K.; Zheng, S. Y.; Yao, L. F.; Zhou, W. Q.; Liu, G. F. Kinetic and thermodynamic aggregation of coordinated supramolecular polymers with quadruple modulated inversion of circular dichroism. *Adv. Opt. Mater.* **2023**, *11*, 2300019.
[41] Fu, K.; Liu, G. F. Multicolor circularly polarized luminescence inversion of metal-organic supramolecular polymers. *Chem. Commun.* **2023**, *59*, 13751–13754.
[42] He, M. L.; Sun, H.; Zhu, L. L.; Liu, G. F. Dynamic circularly polarized luminescence switching of metal-organic supramolecular polymers directed by the competition of solvent-assisted nucleation and thermal nucleation. *Chem. Mater.* **2024**, *36*, 2508–2519.
[43] Fu, K.; Liu, G. F. Full-color circularly polarized luminescence of supramolecular polymers with handedness inversion regulated by anion and temperature. *ACS Nano* **2024**, *18*, 2279–2289.
[44] Fard, M. A.; Behnia, A.; Puddephatt, R. J. Coordination chemistry of mercury(Ⅱ) with 2-pyridylnitrones: Monomers to polymers. *Dalton Trans.* **2017**, *46*, 3579–3587.
[45] Naskar, K.; Maity, S.; Jana, S.; Dutta, B.; Tanaka, S.; Mallick, D.; Akitsu, T.; Sinha, C. Arylazoimidazole coordinated and naphthalene-dicarboxylato bridged polymers of Co(Ⅱ) and photochromic Zn(Ⅱ) complexes. *Cryst. Growth Des.* **2018**, *18*, 2986–2997.
[46] Edington, S. C.; Flanagan, J. C.; Baiz, C. R. An empirical IR frequency map for ester C=O stretching vibrations. *J. Phys. Chem. A* **2016**, *120*, 3888–3896.
[47] Wong, Y. S.; Ng, M.; Yeung, M. C. L.; Yam, V. W. W. Platinum(Ⅱ)-based host–guest coordination-driven supramolecular co-assembly assisted by Pt···Pt and π–π stacking interactions: A dual-selective luminescence sensor for cations and anions. *J. Am. Chem. Soc.* **2021**, *143*, 973–982.
[48] Li, J. J.; Cui, Y. H.; Lu, Y. L.; Zhang, Y. F.; Zhang, K. H.; Gu, C. N.; Wang, K. F.; Liang, Y. J.; Liu, C. S. Programmable supramolecular chirality in non-equilibrium systems affording a multistate chiroptical switch. *Nat. Commun.* **2023**, *14*, 5030.
[49] Romany, A.; Payne, G. F.; Shen, J. Mechanism of the temperature-dependent self-assembly and polymorphism of chitin. *Chem. Mater.* **2023**, *35*, 6472–6481.
[50] Brown, N.; Lei, J. T.; Zhan, C. D.; Shimon, L. J. W.; Adler-Abramovich, L.; Wei, G. H.; Gazit, E. Structural polymorphism in a self-assembled tri-aromatic peptide system. *ACS Nano* **2018**, *12*, 3253–3262.
[51] Boekhoven, J.; Brizard, A. M.; Kowlgi, K. N. K.; Koper, G. J. M.; Eelkema, R.; van Esch, J. H. Dissipative self-assembly of a molecular gelator by using a chemical fuel. *Angew. Chem., Int. Ed.* **2010**, *49*, 4825–4828.
[52] Zhang, L.; Wang, H. X.; Li, S.; Liu, M. H. Supramolecular chiroptical switches. *Chem. Soc. Rev.* **2020**, *49*, 9095–9120.
[53] Kumar, P.; Vo, T.; Cha, M.; Visheratina, A.; Kim, J. Y.; Xu, W. Q.; Schwartz, J.; Simon, A.; Katz, D.; Nicu, V. P. et al. Photonically active bowtie nanoassemblies with chirality continuum. *Nature* **2023**, *615*, 418–424.
[54] Evans, C. G.; O'Brien, J.; Winfree, E.; Murugan, A. Pattern recognition in the nucleation kinetics of non-equilibrium self-assembly. *Nature* **2024**, *625*, 500–507.
[55] Jiang, S. X.; Pal, N.; Hong, F.; Fahmi, N. E.; Hu, H. Y.; Vrbanac, M.; Yan, H.; Walter, N. G.; Liu, Y. Regulating DNA self-assembly dynamics with controlled nucleation. *ACS Nano* **2021**, *15*, 5384–5396.
[56] Zhang, Y. W.; Reinhardt, A.; Wang, P. F.; Song, J.; Ke, Y. G. Programming the nucleation of DNA brick self-assembly with a seeding strand. *Angew. Chem., Int. Ed.* **2020**, *59*, 8594–8600.
[57] Korevaar, P. A.; George, S. J.; Markvoort, A. J.; Smulders, M. M. J.; Hilbers, P. A. J.; Schenning, A. P. H. J.; De Greef, T. F. A.; Meijer, E. W. Pathway complexity in supramolecular polymerization. *Nature* **2012**, *481*, 492–496.
[58] Huang, A. R.; Fan, Y. Y.; Wang, K.; Wang, Z. Z.; Wang, X. Y.; Chang, K.; Gao, Y.; Chen, M. Z.; Li, Q. Q.; Li, Z. Organic persistent RTP crystals: From brittle to flexible by tunable self-partitioned molecular packing. *Adv. Mater.* **2023**, *35*, 2209166.